doi.org/10.1002/batt.202000051

VIP *Very Important Paper*

Special Collection

Slurry-Coated Sulfur/Sulfide Cathode with Li Metal Anode for All-Solid-State Lithium-Sulfur Pouch Cells

Hong Yuan[+],[a, b] Hao-Xiong Nan[+],[a, c] Chen-Zi Zhao[+],[a] Gao-Long Zhu,[a, d] Yang Lu,[a] Xin-Bing Cheng,[a] Quan-Bing Liu,[c] Chuan-Xin He,[d] Jia-Qi Huang,[b] and Qiang Zhang*[a]

All-solid-state lithium-sulfur batteries are strongly considered as the most promising next-generation electrochemical energy storage systems due to their high safety and energy density. However, in view of practical application, it is difficult to obtain large-scale solid-state sulfur cathode continuously. Herein we achieve the large-scale fabrication of solid sulfur cathode by a facile slurry-coating process through the screening of various solvents and binder contents. The composite cathodes in all-solid-state lithium-sulfur pouch cells exhibit a high specific capacity of 1169 mAh g^{-1} and excellent cycling stability. Furthermore, a practical lithium-sulfur pouch cell with an areal discharge capacity of up to 2.3 mAh cm^{-2} is also demonstrated. This work makes a leap towards the practical application of all-solid-state lithium-sulfur batteries.

1. Introduction

Advanced energy storage technologies are attracting extensive attention to meet the ever-growing requirements of energy generation and supply. As the energy density of commercial lithium-ion batteries is reaching the theoretical limit, there is a strong motivation to develop next-generation energy-storage devices with high energy density.[1] Beyond traditional lithium ion batteries, emerging lithium-sulfur (Li–S) batteries are regarded as the most promising next-generation batteries due to its high theoretical energy density of as high as 2600 Wh kg^{-1}.[2] The active material sulfur is also environmental-friendly and earth-abundant. However, the practical Li–S batteries based on routine ether electrolytes are generally hindered by various challenges, such as low sulfur utilization, huge volume expansion, shuttle of polysulfide intermediates, Li dendrite formation, and electrolyte leakage risk.[3]

Recently, the application of solid electrolyte to replace the flammable liquid electrolyte is emerging as an ultimate solution to achieve a safe and high-energy-density device.[4] The utilization of solid electrolytes contributes to solving the safety problems induced by the leakage and explosion of organic electrolytes. The solid-state electrochemical conversion of sulfur (S) and Li_2S avoids the escape of dissolved polysulfides, consequently avoiding the shuttle of polysulfides.[5] Moreover, the Li transference number in solid electrolyte is close to 1, enabling uniform Li metal deposition and inhibiting Li dendrite formation.[6] The rapid development of solid-state fast ionic conductors enables the operation of solid-state batteries, where sulfide inorganic electrolytes constitute a remarkable progress.[7] Their ionic conductivity (~10 mS/cm) even rivals that of liquid organic electrolytes, such as $Li_{10}GeP_2S_{12}$ (LGPS),[8] $Li_{9.54}Si_{1.74}P_{1.44}S_{11.7}Cl_{0.3}$,[9] and Li_6PS_5Cl.[10] However, current solid-state Li–S batteries still suffer from numerous problems. The insulation nature of sulfur requires additional fast electron/ion conductors and binders, which brings about huge challenges in their compatibility.[11] The limited solid-solid point contacts lead to increased interfacial resistance. The electron/ion migration channels can be reduced by the repeated volume changes of active S/Li_2S during charge/discharge process, resulting in retarded electron/ion transportation.

The investigations on all-solid-state Li–S batteries are mainly proceeded in laboratory-scale mould cells with a limited size under high mechanical pressure.[12] On one hand, sulfur cathode can be densified after compaction, rendering well interface contacts between active sulfur, solid electrolyte, and conductive carbon. Therefore, various conductive fillers can be endowed with different dimensions to promote charge transfer at reactive interfaces in sulfur cathode.[13] On the other hand, external mechanical support and fixation can also mitigate the sulfur change in volume upon electrochemical process, maintaining the structural stability and integration of sulfur cathode.

[a] Dr. H. Yuan,[+] Dr. H.-X. Nan,[+] C.-Z. Zhao,[+] Dr. G.-L. Zhu, Dr. Y. Lu, Dr. X.-B. Cheng, Prof. Q. Zhang
Beijing Key Laboratory of Green Chemical Reaction Engineering and Technology
Department of Chemical Engineering
Tsinghua University
Beijing 100084, China
E-mail: zhang-qiang@mails.tsinghua.edu.cn
[b] Dr. H. Yuan,[+] Prof. J.-Q. Huang
Advanced Research Institute of Multidisciplinary Science
Beijing Institute of Technology
Beijing 100081, China
[c] Dr. H.-X. Nan,[+] Prof. Q.-B. Liu
School of Chemical Engineering and Light Industry
Guangdong University of Technology
Guangzhou, 510006, China
[d] Dr. G.-L. Zhu, Prof. C.-X. He
Shenzhen Key Laboratory of Functional Polymer
College of Chemistry and Chemical Engineering
Shenzhen University
Shenzhen, 518000, China
[+] These authors contributed equally to this work.

Supporting information for this article is available on the WWW under https://doi.org/10.1002/batt.202000051

Special Collection An invited contribution to a Special Collection dedicated to Lithium Metal Anode Processing and Interface Engineering.

However, the all-solid-state Li–S batteries should be achieved by scalable processes towards the practical applications.

At present, a dense sulfur cathode by composite powder die compression meets the demands of solid-state batteries on fundamental research. However, it is difficult to achieve a uniform and dense solid electrode at an enlarged size through simply powder densification.[14] One of the reasons is that sulfide electrolytes are unstable at ambient environment, resulting in the failure to obtain higher external mechanical pressure. In general, slurry-coating approach has been regarded as an effective strategy for the large-scale electrode preparation as application in conventional Li–S batteries. Nevertheless, there still remains huge challenges. The reactions between sulfur and sulfides in most of polarity solution result in the destruction of three-phase interface inside cathode and reduced ionic conductivity of sulfide electrolytes. While insolubility of indispensable binders in nonpolar solvent induces unthickened electrode slurry.

In this contribution, large-scale fabrication of sulfur cathode by slurry-coating was achieved for all-solid-state Li–S pouch cells (Figure 1a). After targeted screening of organic solvents with different polarities, the chemical compatibility between sulfur and LGPS electrolyte was firstly demonstrated in n-hexane with weak polarity. Meanwhile, the content of binder was optimized to contribute to the mechanical property of sulfur cathode. Then the sulfur cathode with extended area was prepared by blade coating the slurry on commercial aluminum foil to achieve smooth and flexible electrode (Figure 1b and c). Finally, all-solid-state Li–S pouch cells capable of scaled-up manufacturing were assembled and exhibited excellent electrochemical performances.

2. Results and Discussion

It is well known that slurry-coating is a suitable processing technology for electrode preparation and has been widely applied into the manufacturing of practical lithium-ion batteries.[15] Generally, electrode slurry consists of solvents, active materials, and conductive additives, as well as solid electrolytes for solid batteries. Hence, the primary premise is to ensure structural and functional integrity of active materials and solid electrolytes after this solution process. However, due to their chemical similarity, sulfide electrolytes can react with elemental sulfur to form soluble polysulfides in most organic solvents, especially in polar solvents. Herein LGPS was employed as a representative sulfide electrolyte to investigate the compatibility between sulfur and sulfides in liquid solvents. As shown in Figure 2, some probable solvents, such as tetrahydrofuran, chloroform, xylene, and n-hexane, with low dielectric constants were screened firstly. Although LGPS electrolyte is undissolved into above solvents, unfortunately, it can be seen that sulfur is dissolved into other three solvents except for n-hexane (Figure 2a, b). Moreover, when LGPS and

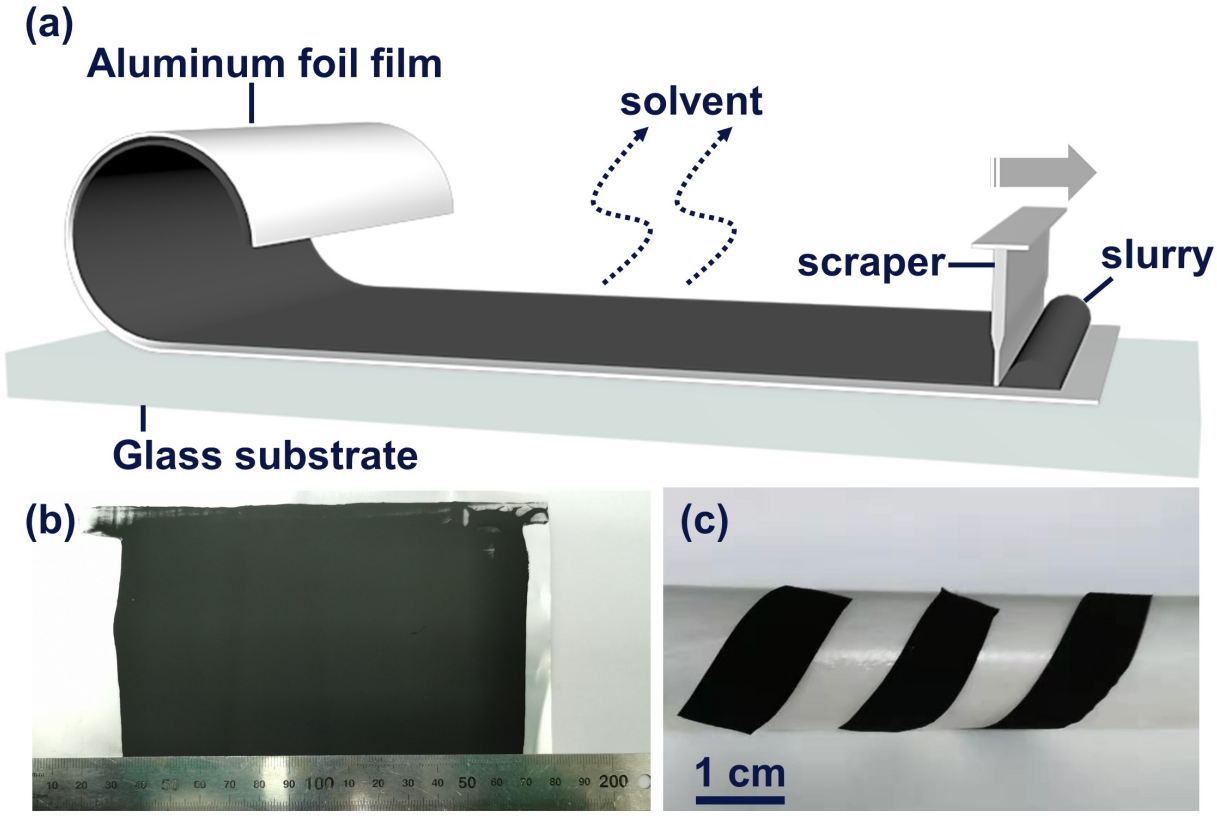

Figure 1. a) Schematic for preparation of solid sulfur electrode film by slurry-coating process. b) Photographs of large-area solid sulfur electrode film on aluminum foil substrate, and c) shows the electrode tailorability and flexibility.

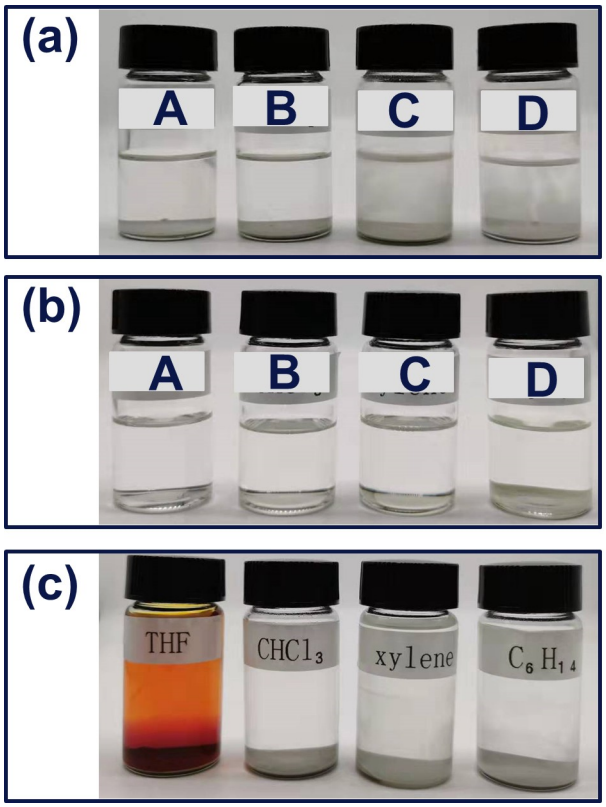

(d)

Sol.	ε	Bp (°C)
A	7.58	66
B	4.81	61
C	2.38	137
D	1.58	69

Figure 2. The solubility of a) S, b) LGPS and c) the reactivity between S and LGPS in various solvents. A, B, C, and D refer to tetrahydrofuran, chloroform, xylene, and n-hexane, respectively.

sulfur coexist, color change is observed in tetrahydrofuran due to relatively high dielectric constant, indicative of serious side reactions between LGPS and sulfur to form polysulfides (Figure 2c, d). This side reaction not only destructs ionic conduction of sulfide electrolyte but also alters sulfur electrochemistry. Therefore, n-hexane is regarded as a target dispersion solvent for slurry process.

In order to further confirm the availability of n-hexane, X-ray powder diffraction (XRD) patterns were conducted. As shown in Figure 3a, the characteristic peaks attributed to LGPS at $2\theta = 29.7°$, 41.5°, and 47.5° are remained after n-hexane immersion treatment, implying no destruction of LGPS crystal structure.[16] The ionic conductivity (3.8 mS cm^{-1}) of LGPS after soaking also has no obvious reduction compared with that (3.9 mS cm^{-1}) of pristine LGPS (Figure S1). Moreover, sulfur and LGPS diffraction peaks are clearly demonstrated for LGPS/sulfur composites simultaneously, which further prove the compatibility between solid electrolyte and S in n-hexane.

In addition, appropriate viscosity and dispersion of slurry are also critical for high-quality solid electrode preparation. Considering the compatibility with low polarity n-hexane solvent, silicone rubber (SR) can serve as a thickener to regulate the viscosity and dispersion of solution slurry. Meanwhile, SR as a macromolecular polymer is capable of conglutinating electrode materials onto conductive substrate and maintaining structural integrity and stability upon cycling. More importantly, SR with granular domain structure is incapable of completely covering the surface of the solid electrode particles.[17] Thus, SR binders just have limited effects on the interface ionic/electronic transportation between solid sulfur and solid electrolyte, as well as conductive carbon.[18] Therefore, SR was applied as a binder and a thickener to regulate slurry properties. The binder content optimizations are discussed in detail in the below section. Solid sulfur electrode films composed of sulfur, LGPS, carbon nanotube, and 2 wt.% SR, were prepared by a slurry-coating process. Sulfur electrode films exhibit smooth surface with uniform particle size distribution (Figure 3b). Furthermore, energy dispersion spectra (EDS) element mapping (Figure 3d) demonstrate that C, S, P, and Si are distributed in the composite cathode uniformly. Manipulating the height of scraper, the thickness and sulfur loading of electrode can be controlled. As shown in Figure 3c, the thickness of cathode film is 130 μm and the sulfur loading is 1.3 mg cm^{-2}.

In order to investigate the effect of SR binder content in solid sulfur cathode on reaction kinetics, cyclic voltammogram (CV) measurements were performed in a mould battery under compression at 60 °C (Figure 4a). This battery configuration consists of Li–In alloy as anode, thickened LGPS pellet with the original particle size of about 0.2–2.0 μm (Figure S2) as electrolyte and as-prepared solid sulfur electrode film as cathode. Li–In alloy applied for replacing Li anode is to mitigate the side reaction between Li metal and LGPS and thus to construct a stable anode/sulfide interface. The peaks around 1.1 and 1.9 V are attributed to S oxidation and Li_2S reduction, respectively,

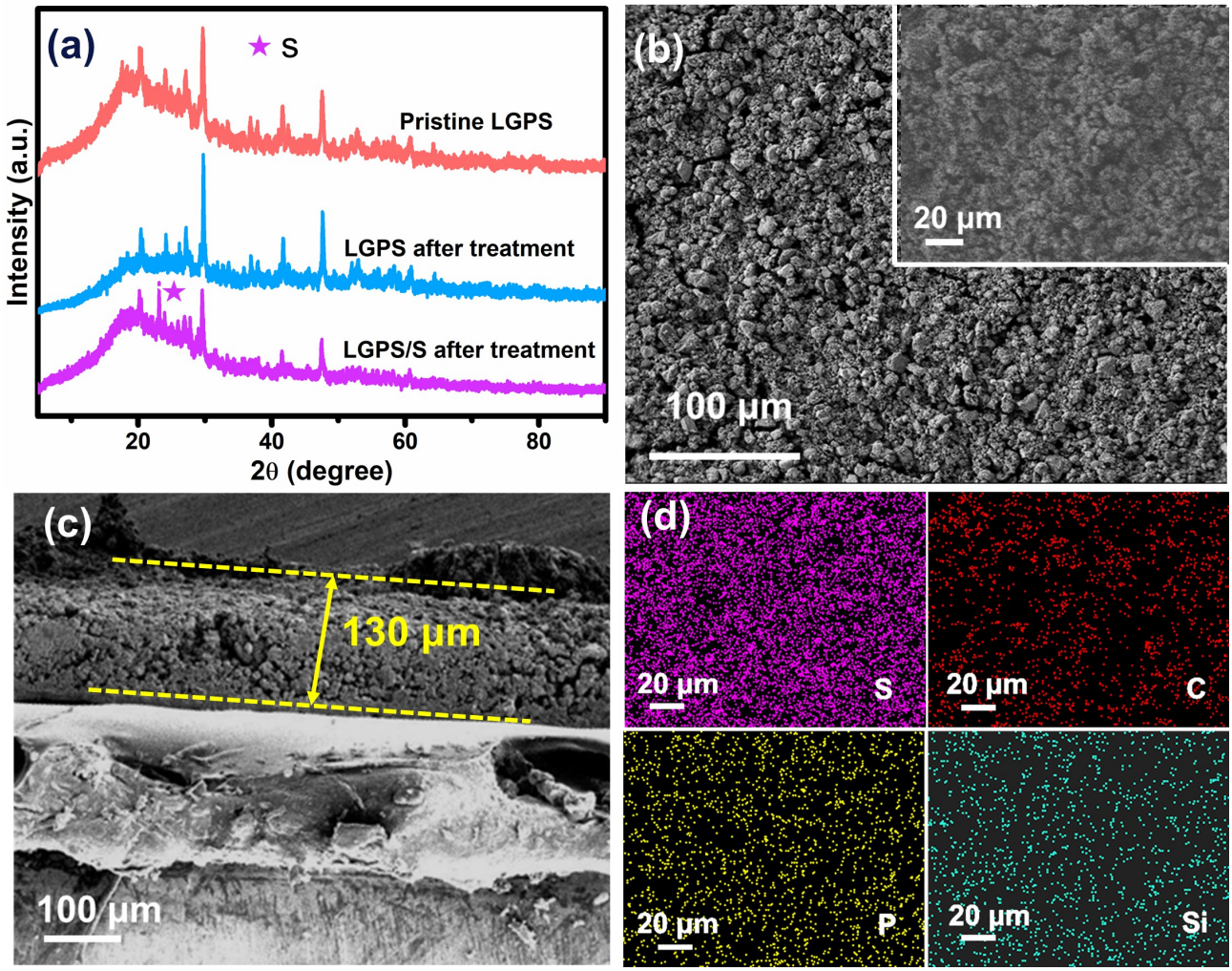

Figure 3. a) XRD patterns of pristine LGPS, LGPS after n-hexane treatment and LGPS/S composite after n-hexane treatment. b) Surface morphology images, c) cross section image, and d) corresponding EDS elemental mapping images of solid sulfur electrode films with 2 wt.% SR binder. Inset of (b) is the enlarged SEM image.

exhibiting the reversible electrochemical redox conversion between S and Li_2S. With the increase of binder content in the solid sulfur cathode, the redox peak current reduces, indicating that the excess inactive SR binder is not conducive to sulfur reaction kinetics. To quantitatively reveal the effect of SR binder on reaction kinetics, Tafel polarization was performed. As shown in Figure S4, solid electrode with 2 wt.% SR exhibits the lowest Tafel slope (211.2 mV dec^{-1} for reduction; 264.3 mV dec^{-1} for oxidation). Moreover, Tafel slopes of the solid cathode increase with elevated SR content. When SR content increases to 10 wt.%, Tafel slope reaches to the maximum (304.8 mV dec^{-1} for reduction; 295.6 mV dec^{-1} for oxidation). Theoretically, inactive SR binder is adverse to contributing to charge transportation. However, in addition to be imperative for cathode slurry thickening, SR binder not only binds electrodes onto conductive substrates but also maintains electrode stability and avoids electrode cracking. Therefore, SR content of 2 wt.% is comprehensively considered as a reasonable amount of binder for solid sulfur electrode manufacturing by slurry process.

Galvanostatic discharge-charge measurements were conducted to evaluate the electrochemical performances of solid sulfur electrode films. It can be obviously seen discharge/charge profiles with typical single plateau, which suggests immediately solid conversion between S and Li_2S (Figure 4b). Moreover, the highest initial discharge capacity of 988.1 mAh g^{-1} is observed for solid electrode films with 2 wt.% SR binder and 1.3 mg cm^{-2} S loading. The discharge capacity reduces with the rise of binder content. When the SR content increases to 10 wt.%, an initial discharge capacity of only 704.1 mAh g^{-1} is obtained, which is mainly attributed to the reduced charge transfer capabilities with the increase of an inactive SR binder. As a contrast, conventional C/S/LGPS composite cathode tablets were constructed by powder die compression. An initial discharge capacity of 1031.9 mAh g^{-1} for this composite cathode is achieved. The discharge capacity for solid electrode film with 2 wt.% SR just reduces by 4.2% compared with C/S/LGPS composite cathode (Figure S5), indicating that sulfur electrochemical conversion is barely affected by negligible SR binder. Electrochemical impedance

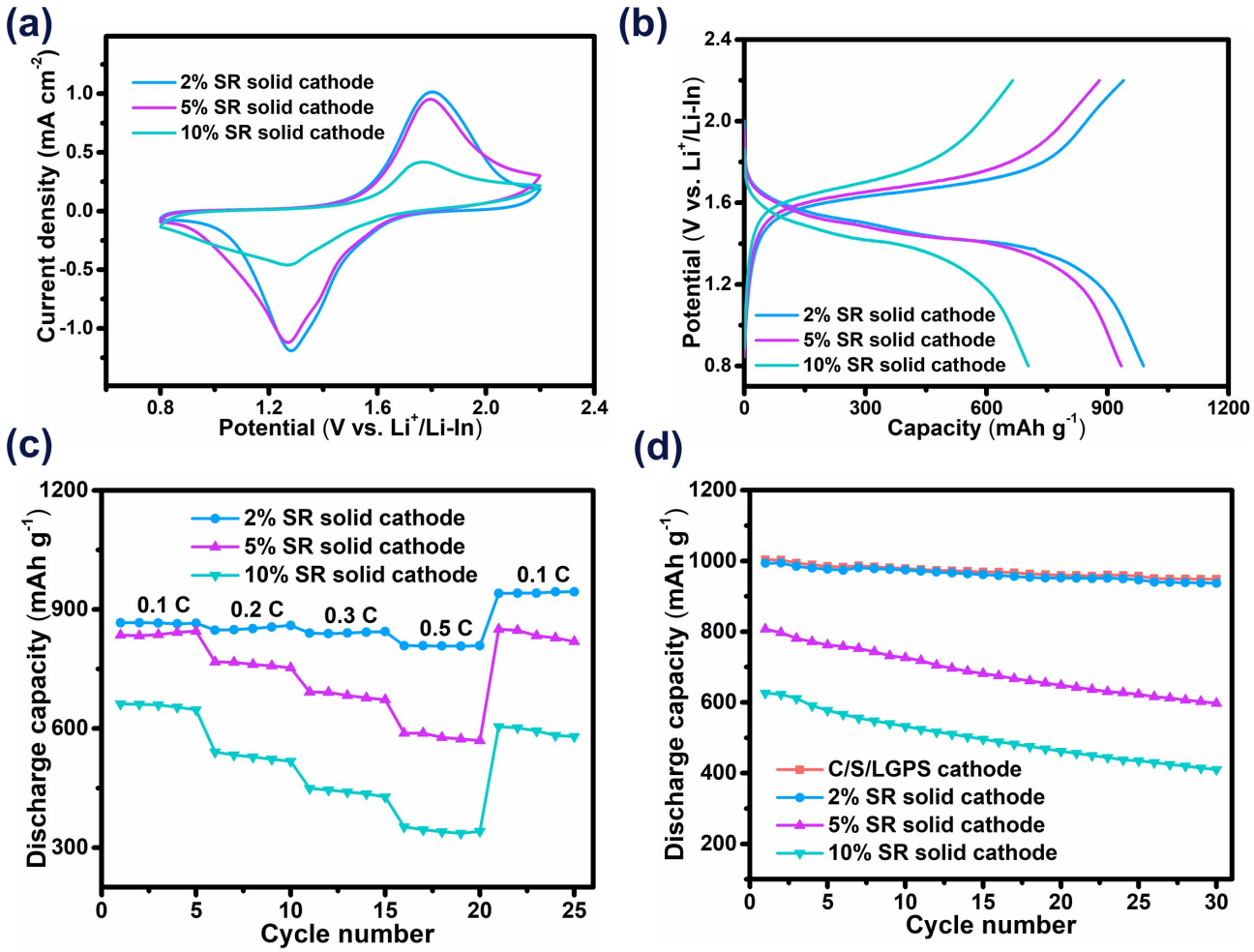

Figure 4. a) CV curves, b) voltage-capacity curves at 0.05 C, c) rate capabilities, and d) the cycle performances at 0.21 mA cm^{-2} (0.1 C) of solid sulfur electrode with different SR content. The sulfur loading is 1.3 mg cm^{-2}.

spectra further confirm the insignificant influences on charge transfer capability in a solid electrode film (Figure S6).

The rate capacity strongly relies on interfacial charge transportation. To further prove the feasibility of solid electrode by slurry-coating process in practical batteries, the electrochemical performances at different rates were evaluated. As shown in Figure 4c, solid electrodes with 2 wt.% SR exhibit discharge capacity of 865.5, 860.0, 844.4, and 808.7 mAh g^{-1} at 0.1, 0.2. 0.3 and 0.5 C, respectively. Notably, an enhanced capacity of 944.8 mAh g^{-1} is obtained when returns to at 0.1 C after high rate tests, which is even higher than initial discharge capacity. While solid electrode with 5 wt.% SR shows a rapidly reduced discharge capacity of just 569.7 mAh g^{-1} at 0.5 C, suggesting aggravated charge transfer impedance owing to increased SR content. In contrast, traditional C/S/LGPS composite cathode delivers a rapid rate capacity decay from 1008.0 mAh g^{-1} at 0.1 C to 851.9 mAh g^{-1} at 0.5 C. Theoretically, the rate capabilities should be reduced due to the presence of inactive SR binder. However, a higher capacity retention at enhanced rate and a higher capacity recovery for 2 wt.% SR solid electrode are observed, which is attributed to the melting of SR at elevated temperature of 60 °C and thus contributed to enhanced Li ion transportation.

The cycling stability also reveals the feeble effect of SR (Figure 4d). After activation at a low initial rate, a specific capacity of 983.5 mAh g^{-1} is exhibited for 2 wt.% SR solid electrode after initial discharge at 0.1 C. Moreover, a high reversible capacity of 937.2 mAh g^{-1} is reserved after continuous 30 cycles, which is comparable to that of conventional C/S/LGPS composite powder cathode. In contrast, the discharge capacity for solid electrode with 5 wt.% SR decreases by 19.7% after just 20 cycles due to possibly limited charge transfer. These results further proved the availability of 2 wt.% SR solid electrode constructed by a slurry-coating process.

In terms of practical application, pouch cells are generally utilized as the main battery configuration and widely applied in the field of power battery manufacturing. In terms of an enlarged all-solid-state pouch cell, however, interface problems will be aggravated in comparison to that in a mould cell. In order to investigate the practicability of solid sulfur cathode by slurry coating, all-solid-state Li–S pouch cells with a size of 30 × 30 mm^2 were fabricated (Figure 5a). In view of the voltage drop using Li–In alloy anode, lithium metal with a thickness of

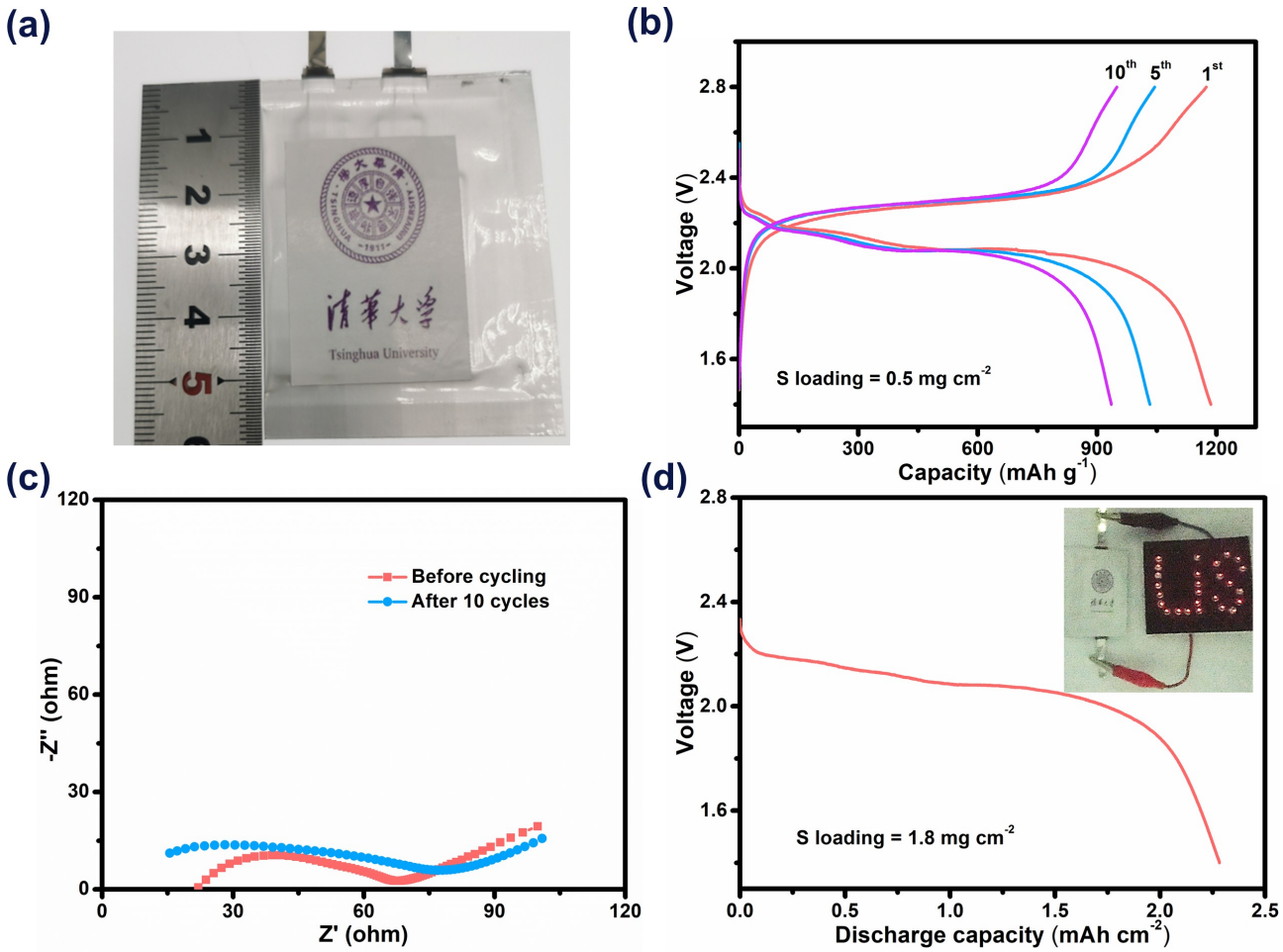

Figure 5. a) Optical photograph and b) the charge-discharge voltage profiles of all-solid-state Li–S pouch cells with 2 wt.% SR content solid electrode at 0.01 C, and c) their EIS profiles before and after cycling. d) The discharge profile of the pouch cells with 1.8 mg cm^{-2} sulfur loading, inset is the optical photograph of illumined Li–S shape red diodes by pouch cell.

100 μm was adopted as anodes; while Li_6PS_5Cl was selected as ionic conductor layers due to the compatibility between Li and Li_6PS_5Cl.[19] As shown in Figure 5b, the pouch cell with 0.5 mg cm^{-2} sulfur loading exhibits a high discharge capacity of 1169 mAh g^{-1} at 0.01 C at 60 °C. Even after 10 cycles, a reversible capacity of up to 950 mAh g^{-1} is reserved. Moreover, even if in a pouch cell, the interface impedances at initial state and after 10 cycles is still below 70 Ω, indicating structural stability and interfacial integrity of solid electrode by coating (Figure 5c). In consideration of the requirement for high energy density, sulfur electrode with a higher sulfur loading of 1.8 mg cm^{-2} was prepared, and an areal capacity of more than 2.3 mAh cm^{-2} was gained, exhibiting huge potentials in practical application (Figure 5d). Meanwhile, typical single discharge/charge plateau also proves the solid-phase sulfur conversion. At the same time, attributed to elevated cell voltage derived from the use of lithium anode, Li–S shape red light emitting diodes were illuminated continuously.

Theoretically, high energy density can be gained if reducing the solid electrolyte thickness. Nevertheless, present research aims to reveal the effectiveness of practical slurry coating process in the large-scale fabrication of solid sulfur electrode. In order to further promote the development of practical all-solid-state Li–S batteries, the preparation of solid electrolyte layers by appropriate industrial process can also be considered in future research. Therefore, a cathode supported electrolyte layer by similar slurry coating is a promising approach. More importantly, this method only requires smaller amount of solid electrolyte to obtain a thinner solid electrolyte layer.

3. Conclusions

A slurry-coating method is applied to the large-scale fabrication of solid sulfur cathode for all-solid-state Li–S batteries. The effects of dispersion solvents with different polarity on the structure and morphology of active sulfur and sulfide electrolyte were investigated. Thus, n-hexane with weak polarity and low dielectric constant was screened out to achieve the compatibility between sulfur and sulfides electrolyte in dispersion solvent. Considering the structural stability and interfacial charge transfer impedance, the optimized binder content of 2 wt.% in solid sulfur electrode was demonstrated and exhibited excellent electrochemical performances. Finally, all-

solid-state Li–S pouch cells with a size of $30\times30\ mm^2$ were successfully assembled. The pouch cells exhibited an initial discharge capacity of 1169 $mAh\,g^{-1}$ at 0.01 C and high capacity retention of 950 $mAh\,g^{-1}$ after 10 cycles. Furthermore, a high practical areal capacity of as high as 2.3 $mAh\,cm^{-2}$ was also confirmed. This work makes a leap towards the practical application of all-solid-state Li–S batteries and affords more fundamental understandings based on practical solid-state pouch cells.

Experimental Section

Preparation of solid sulfur electrode by slurry coating

The conventional $C/S/Li_{10}GeP_2S_{12}$ composites were firstly prepared referring to our previous work.[20] 1.96 g C/S/LGPS composites, 0.4 g 10% of silicone rubber (SR) n-hexane solution and 5 mL n-hexane were mixed and sealed in a ZrO_2 ball milling tank. After ball milling with a rotation speed of 600 rpm for 8 hours, the slurry with 2 wt.% SR was gained. After that the solid electrodes were prepared by coating above-obtained sulfur slurry on Al foil substrates. The sulfur loading was controlled by a height regulator scraper. The above experiments were operated in a glove box. For comparison, the solid sulfur electrodes with different SR contents were also fabricated through the same approach.

Cell assembly

Mould cell: Fundamental electrochemical performances of solid sulfur electrode were investigated in a poly(ether-ether-ketone) (PEEK) mold cell with a diameter of 10 mm. Firstly, 100 mg of LGPS was pressed into a tablet as the solid electrolyte (SE) layer at 360 MPa. Then, solid sulfur electrode film was located at one side of SE and compressed at 360 MPa. Lithium–indium (Li–In) alloy was attached to the opposite side of the SE layer. Finally, a mould cell was assembled.

Preparation of electrolyte sheet for pouch cell: As for all-solid-state Li–S pouch cells, lithium metal with the thickness of 100 μm was employed as anodes; while Li_6PS_5Cl was selected as ionic conductor layers due to the compatibility between Li and Li_6PS_5Cl. In detail, Li_6PS_5Cl with the original particle size of about 0.2–2.0 μm (Figure S2), nitrile rubber, and chloroform were mixed with a certain mass ratio and sealed in a ZrO_2 ball milling tank. After ball milling with rotation speed of 600 rpm for 8 hours, a uniformly dispersed slurry was gained. The slurry was taken in a $33\times33\ mm^2$ stainless steel mold. After drying and being pressed at 300 MPa, an electrolyte sheet was prepared with the thickness of 380 μm. The electrolyte sheet preparation procedures were all performed in an Ar glove box.

All-solid-state Li–S Pouch cell: The pressed electrolyte sheet was placed in a $33\times33\ mm^2$ stainless steel mold. A $30\times30\ mm^2$ sulfur electrode sheet was cut and placed on the electrolyte sheet and compressed at 300 MPa. Then a lithium negative electrode was pasted on the opposite side of the SE sheet. Finally, the lugs were led out, and the Al plastic film was encapsulated to complete the assembly of pouch cell. The thickness of the pouch cell with 0.5 $mg\,cm^{-2}$ sulfur loading is 840 μm. The above processes were performed in a dry room with a dew point of −40 °C.

Material characterization

X-ray powder diffraction (XRD) patterns were conducted on an X-ray powder diffractometer (D8 Advance, Bruker) equipped with filtered Cu–K_α radiation operating at 30 kV and 20 mA. Scanning electron microscopy (SEM) images and corresponding energy-dispersive X-ray analysis (EDX) were obtained on JSM 7401F (JEOL, Japan).

Electrochemical characterization

Cyclic voltammetry (CV) of all-solid-state cells was measured with a scan rate of 0.1 $mV\,s^{-1}$ on an electrochemical workstation (Solartron, 1470E). Electrochemical impedance spectra (EIS) measurements were performed using the same workstation with an amplitude of 10 mV over the frequency range from 10^6 Hz to 0.1 Hz. Galvanostatic charge-discharge tests were carried out on LAND multichannel battery cycler (Wuhan LAND Electronics Co., Ltd.).

Acknowledgements

This work was supported by National Key Research and Development Program (2016YFA0202500 and 2016YFA0200102), National Natural Science Foundation of China (21676160, 21808124, 21905056, and U1801257), and China Postdoctoral Science Foundation (2019T120098).

Conflict of Interest

The authors declare no conflict of interest.

Keywords: all-solid-state lithium-sulfur batteries · sulfide solid electrolyte · slurry-coating process · pouch cells · composite electrode

[1] a) Z. P. Cano, D. Banham, S. Ye, A. Hintennach, J. Lu, M. Fowler, Z. Chen, *Nat. Energy* **2018**, *3*, 279–289; b) X.-B. Cheng, C. Yan, X. Chen, C. Guan, J.-Q. Huang, H.-J. Peng, R. Zhang, S.-T. Yang, Q. Zhang, *Chem* **2017**, *2*, 258–270; c) X.-B. Cheng, R. Zhang, C.-Z. Zhao, Q. Zhang, *Chem. Rev.* **2017**, *117*, 10403–10473; d) Y. Zhao, K. R. Adair, X. Sun, *Energy Environ. Sci.* **2018**, *11*, 2673–2695; e) Y. Liang, C.-Z. Zhao, H. Yuan, Y. Chen, W. Zhang, J.-Q. Huang, D. Yu, Y. Liu, M.-M. Titirici, Y.-L. Chueh, H. Yu, Q. Zhang, *InfoMat* **2019**, *1*, 6–32; f) L. Jiang, X.-B. Cheng, H.-J. Peng, J.-Q. Huang, Q. Zhang, *eTransportation* **2019**, *2*, 100033.

[2] a) Z. W. Seh, Y. Sun, Q. Zhang, Y. Cui, *Chem. Soc. Rev.* **2016**, *45*, 5605–5634; b) A. Manthiram, S.-H. Chung, C. Zu, *Adv. Mater.* **2015**, *27*, 1980–2006; c) H.-J. Peng, J.-Q. Huang, X.-B. Cheng, Q. Zhang, *Adv. Energy Mater.* **2017**, *7*, 1700260; d) X. Liang, J. Yun, K. Xu, H. Xiang, Y. Wang, Y. Sun, Y. Yu, *J. Energy Chem.* **2019**, *39*, 176–181; e) Q. Sun, K. C. Lau, D. Geng, X. Meng, *Batteries* **2018**, *1*, 41–68; f) H. Tang, W. Li, L. Pan, C. P. Cullen, Y. Liu, A. Pakdel, D. Long, J. Yang, N. McEvoy, G. S. Duesberg, V. Nicolosi, C. Zhang, *Adv. Sci.* **2018**, *5*, 1800502; g) H. Tang, W. Li, L. Pan, K. Tu, F. Du, T. Qiu, J. Yang, C. P. Cullen, N. McEvoy, C. Zhang, *Adv. Funct. Mater.* **2019**, *29*, 1901907.

[3] a) L. Kong, X. Chen, B.-Q. Li, H.-J. Peng, J.-Q. Huang, J. Xie, Q. Zhang, *Adv. Mater.* **2018**, *30*, 1705219; b) Q. Pang, X. Liang, C. Y. Kwok, J. Kulisch, L. F. Nazar, *Adv. Energy Mater.* **2017**, *7*, 1601630; c) B.-Q. Li, L. Kong, C.-X. Zhao, Q. Jin, X. Chen, H.-J. Peng, J.-L. Qin, J.-X. Chen, H. Yuan, Q. Zhang, J.-Q. Huang, *InfoMat* **2019**, *1*, 533–541; d) X. Tao, J. Wang, C. Liu, H. Wang, H. Yao, G. Zheng, Z. W. Seh, Q. Cai, W. Li, G. Zhou, C. Zu, Y. Cui, *Nat. Commun.* **2016**, *7*, 11203; e) H. Yuan, H.-J. Peng,

B.-Q. Li, J. Xie, L. Kong, M. Zhao, X. Chen, J.-Q. Huang, Q. Zhang, *Adv. Energy Mater.* **2019**, *9*, 1802768; f) B.-Q. Li, H.-J. Peng, X. Chen, S.-Y. Zhang, J. Xie, C.-X. Zhao, Q. Zhang, *CCS* **2019**, *1*, 128–137; g) B. Krüner, T. S. Dörr, H. Shim, J. Sann, J. Janek, V. Presser, *Batteries* **2018**, *1*, 83–94; h) X. Li, M. Banis, A. Lushington, X. Yang, Q. Sun, Y. Zhao, C. Liu, Q. Li, B. Wang, W. Xiao, C. Wang, M. Li, J. Liang, R. Li, Y. Hu, L. Goncharova, H. Zhang, T.-K. Sham, X. Sun, *Nat. Commun.* **2018**, *9*, 4509.

[4] a) J. Yue, M. Yan, Y.-X. Yin, Y.-G. Guo, *Adv. Funct. Mater.* **2018**, *28*, 1707533; b) Y. Lu, S. Gu, X. Hong, K. Rui, X. Huang, J. Jin, C. Chen, J. Yang, Z. Wen, *Energy Storage Mater.* **2018**, *11*, 16–23; c) R. Xu, S. Zhang, X. Wang, Y. Xia, X. Xia, J. Wu, C. Gu, J. Tu, *Chem. Eur. J.* **2018**, *24*, 6007–6018; d) L. Xu, S. Tang, Y. Cheng, K. Wang, J. Liang, C. Liu, Y.-C. Cao, F. Wei, L. Mai, *Joule* **2018**, *2*, 1991–2015; e) Z. Fan, B. Ding, T. Zhang, Q. Lin, V. Malgras, J. Wang, H. Dou, X. Zhang, Y. Yamauchi, *Small* **2019**, *15*, 1903952; f) S. Xia, X. Wu, Z. Zhang, Y. Cui, W. Liu, *Chem* **2019**, *5*, 753–785; g) L. Chen, L.-Z. Fan, *Energy Storage Mater.* **2018**, *15*, 37–45; h) M. Zhu, J. Wu, Y. Wang, M. Song, L. Long, S. H. Siyal, X. Yang, G. Sui, *J. Energy Chem.* **2019**, *37*, 126–142; i) L. Meabe, N. Goujon, C. Li, M. Armand, M. Forsyth, D. Mecerreyes, *Batteries* **2020**, *3*, 68–75; j) J. Bae, Y. Li, J. Zhang, X. Zhou, F. Zhao, Y. Shi, J. B. Goodenough, G. Yu, *Angew. Chem. Int. Ed.* **2018**, *57*, 2096–2100; *Angew. Chem.* **2018**, *130*, 2118–2112.

[5] a) K. Fu, Y. Gong, G. T. Hitz, D. W. McOwen, Y. Li, S. Xu, Y. Wen, L. Zhang, C. Wang, G. Pastel, J. Dai, B. Liu, H. Xie, Y. Yao, E. D. Wachsman, L. Hu, *Energy Environ. Sci.* **2017**, *10*, 1568–1575; b) P. Zhu, C. Yan, J. Zhu, J. Zang, H. Jia, X. Dong, Z. Du, C. Zhang, N. Wu, M. Dirican, X. Zhang, Y. Li, *Energy Storage Mater.* **2019**, *17*, 220–225.

[6] a) Y.-Z. Sun, J.-Q. Huang, C.-Z. Zhao, Q. Zhang, *Sci. China Chem.* **2017**, *60*, 1508–1526; b) A. Manthiram, X. Yu, S. Wang, *Nat. Rev. Mater.* **2017**, *2*, 16103; c) S. Xin, Y. You, S. Wang, H.-C. Gao, Y.-X. Yin, Y.-G. Guo, *ACS Energy Lett.* **2017**, *2*, 1385–1394; d) X. Shen, X. Cheng, P. Shi, J. Huang, X. Zhang, C. Yan, T. Li, Q. Zhang, *J. Energy Chem.* **2019**, *37*, 29–34; e) X. Q. Zhang, C. Z. Zhao, J. Q. Huang, Q. Zhang, *Engineering* **2018**, *4*, 831–847.

[7] a) K. H. Park, Q. Bai, D. H. Kim, D. Y. Oh, Y. Zhu, Y. Mo, Y. S. Jung, *Adv. Energy Mater.* **2018**, *8*, 1800035 ; b) C. Yu, S. Ganapathy, E. R. H. van Eck, L. van Eijck, N. de Klerk, E. M. Kelder, M. Wagemaker, *J. Energy Chem.* **2019**, *38*, 1–7; c) C. Luo, X. Ji, J. Chen, K. J. Gaskell, X. He, Y. Liang, J. Jiang, C. Wang, *Angew. Chem. Int. Ed.* **2018**, *57*, 8567–8571; *Angew. Chem.* **2018**, *130*, 8703–8707; d) Y. Wang, X. Lu, C. Zheng, X. Liu, Z. Chen, W. Yang, J. Lin, F. Huang, *Angew. Chem. Int. Ed.* **2019**, *58*, 7673–7677; *Angew. Chem.* **2019**, *131*, 7755–7759; e) E. Umeshbabu, B. Zheng, Y. Yang, *Electrochem. Energy Rev.* **2019**, *2*, 199–230.

[8] a) N. Kamaya, K. Homma, Y. Yamakawa, M. Hirayama, R. Kanno, M. Yonemura, T. Kamiyama, Y. Kato, S. Hama, K. Kawamoto, A. Mitsui, *Nat. Mater.* **2011**, *10*, 682–686; b) E. Umeshbabu, B. Zheng, J. Zhu, H. Wang, Y. Li, Y. Yang, *ACS Appl. Mater. Interfaces* **2019**, *11*, 18436–18447; c) X. Yao, N. Huang, F. Han, Q. Zhang, H. Wan, J. P. Mwizerwa, C. Wang, X. Xu, *Adv. Energy Mater.* **2017**, *7*, 1602923.

[9] a) Y. Kato, S. Hori, T. Saito, K. Suzuki, M. Hirayama, A. Mitsui, M. Yonemura, H. Iba, R. Kanno, *Nat. Energy* **2016**, *1*, 16030; b) Q. Zhang, D. Cao, Y. Ma, A. Natan, P. Aurora, H. Zhu, *Adv. Mater.* **2019**, *31*, 1901131.

[10] a) H.-J. Deiseroth, S.-T. Kong, H. Eckert, J. Vannahme, C. Reiner, T. Zaiss, M. Schlosser, *Angew. Chem. Int. Ed.* **2008**, *47*, 755–758; *Angew. Chem.* **2008**, *120*, 767–770; b) F. Han, J. Yue, X. Fan, T. Gao, C. Luo, Z. Ma, L. Suo, C. Wang, *Nano Lett.* **2016**, *16*, 4521–4527; c) L. Zhou, K.-H. Park, X. Sun, F. Lalère, T. Adermann, P. Hartmann, L. F. Nazar, *ACS Energy Lett.* **2019**, *4*, 265–270.

[11] a) H. Yuan, H.-J. Peng, J.-Q. Huang, Q. Zhang, *Adv. Mater. Interfaces* **2019**, *6*, 1802046; b) S. Chen, D. Xie, G. Liu, J. P. Mwizerwa, Q. Zhang, Y. Zhao, X. Xu, X. Yao, *Energy Storage Mater.* **2018**, *14*, 58–74; c) W. Li, Q. Wang, J. Jin, Y. Li, M. Wu, Z. Wen, *Energy Storage Mater.* **2019**, *23*, 299–305.

[12] a) J.-M. Doux, N. Han, D. H. S. Tan, A. Banerjee, X. Wang, E. A. Wu, C. Jo, H. Yang, Y. S. Meng, *Adv. Energy Mater.* **2020**, *10*, 1903253; b) H. Zheng, S. Wu, R. Tian, Z. Xu, H. Zhu, H. Duan, H. Liu, *Adv. Funct. Mater.* **2020**, *30*, 1906189; c) Q. Zhang, N. Huang, Z. Huang, L. Cai, J. Wu, X. Yao, *J. Energy Chem.* **2020**, *40*, 151–155.

[13] a) Y. Zhang, T. Liu, Q. Zhang, X. Zhang, S. Wang, X. Wang, L. Li, L.-Z. Fan, C.-W. Nan, Y. Shen, *J. Mater. Chem. A* **2018**, *6*, 23345–23356; b) A. Sakuda, Y. Sato, A. Hayashi, M. Tatsumisago, *Energy Technol.* **2019**, *7*, 1900077.

[14] a) T. Ates, M. Keller, J. Kulisch, T. Adermann, S. Passerini, *Energy Storage Mater.* **2019**, *17*, 204–210; b) A. Sakuda, K. Kuratani, M. Yamamoto, M. Takahashi, T. Takeuchi, H. Kobayashi, *J. Electrochem. Soc.* **2017**, *164*, A2474-A2478; c) X. Yang, J. Luo, X. Sun, *Chem. Soc. Rev.* **2020**, *49*, 2140-2195 ; d) X. Yang, X. Li, K. Adair, H. Zhang, X. Sun, *Electrochem. Energy Rev.* **2018**, *1*, 239–293.

[15] X. Yang, Y. Chen, M. Wang, H. Zhang, X. Li, H. Zhang, *Adv. Funct. Mater.* **2016**, *26*, 8427–8434.

[16] a) Q. Zhang, H. Wan, G. Liu, Z. Ding, J. P. Mwizerwa, X. Yao, *Nano Energy* **2019**, *57*, 771–782; b) Z. Zhang, S. Chen, J. Yang, J. Wang, L. Yao, X. Yao, P. Cui, X. Xu, *ACS Appl. Mater. Interfaces* **2018**, *10*, 2556–2565.

[17] T. Inada, K. Takada, A. Kajiyama, M. Kouguchi, H. Sasaki, S. Kondo, M. Watanabe, M. Murayama, R. Kanno, *Solid State Ionics* **2003**, *158*, 275–280.

[18] T. Inada, K. Takada, A. Kajiyama, H. Sasaki, S. Kondo, M. Watanabe, M. Murayama, R. Kanno, *J. Power Sources* **2003**, *119*, 948–950.

[19] X. Chi, Y. Liang, F. Hao, Y. Zhang, J. Whiteley, H. Dong, P. Hu, S. Lee, Y. Yao, *Angew. Chem. Int. Ed.* **2018**, *57*, 2630–2634; *Angew. Chem.* **2018**, *130*, 2660–2664.

[20] L.-P. Hou, H. Yuan, C.-Z. Zhao, L. Xu, G.-L. Zhu, H.-X. Nan, X.-B. Cheng, Q.-B. Liu, C.-X. He, J.-Q. Huang, Q. Zhang, *Energy Storage Mater.* **2020**, *25*, 436–442.

Manuscript received: March 11, 2020
Revised manuscript received: March 28, 2020
Accepted manuscript online: March 29, 2020
Version of record online: ■■, ■■■

ARTICLES

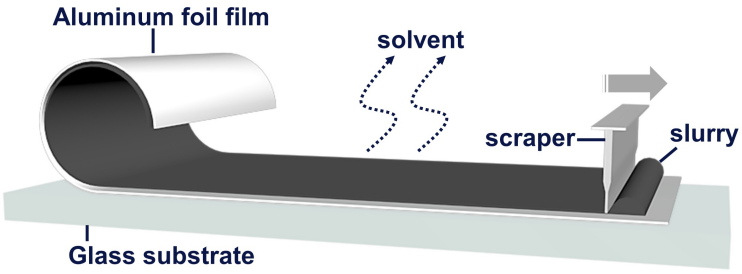

Slurry coated sulfur/sulfide cathode for all-solid-state Li–S pouch cells

Next-generation cathodes: The large-scale fabrication of solid sulfur/sulfide cathode is successfully achieved for all-solid-state lithium-sulfur pouch cells by a facile slurry-coating process and thus, exhibiting excellent electrochemical performances.